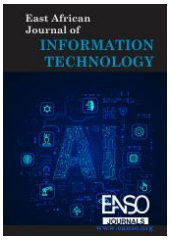

East African Journal of Information Technology
eajit.eanso.org
Volume 7, Issue 1, 2024
Print ISSN: 2707-5346 | Online ISSN: 2707-5354
Title DOI: https://doi.org/10.37284/2707-5354

EAST AFRICAN NATURE & SCIENCE ORGANIZATION

Original Article

Effect of BaTiO3 and Chitosan Composite Material on the Enhancement of the Sensitivity and Limit of Detection of the Surface Plasmon Resonance Sensor-Divergent Beam Based

Jordan H. Hossea[1*]

[1] Dar es Salaam Institute of Technology, P. O. Box 2958, Dar es Salaam, Tanzania.
* Author's Email: jordan.hossea@dit.ac.tz

Article DOI: https://doi.org/10.37284/eajit.7.1.2463

Date Published: *29 November 2024*

Keywords: *Divergence Beam, SPR Sensor, Limit of Detection (LOD), Chitosan and Sensitivity.*

ABSTRACT

The SPR sensor's poor sensitivity and low limit of detection (LOD) limit its use for tiny contamination detection when the measured sample ranges from 1.3317 to 34. Thus, study examined the combined influence of CaF2/ZnO/TiO2/Silver/BaTiO3/Chitosan on the performance of an SPR biosensor employing the Kretschman configuration. The proposed SPR sensor use the Kretschmann configuration, which employs the divergence beam produced by the Powell lens to avoid mechanical rotation. Through the use of an STM32F401RE controller with 12-bit ADC, it was determined that the proportionate alloying of BaTiO3 and chitosan with optimal thickness could enhance the designed SPR sensor's theoretical sensitivity to 480.45˚/RIU and limit of detection (LOD) to. Thus proposed SPR sensor showed the improvement in sensitivity and LOD by 16.67% and 33.69%, respectively, as compared to the SPR sensor without the combined effect of optimal chitosan and BaTiO3 thickness.

APA CITATION

Hossea, J. H. (2024). Effect of BaTiO3 and Chitosan Composite Material on the Enhancement of the Sensitivity and Limit of Detection of the Surface Plasmon Resonance Sensor-Divergent Beam Based. *East African Journal of Information Technology*, *7*(1), 412-426. https://doi.org/10.37284/eajit.7.1.2463

CHICAGO CITATION

Hossea, Jordan H. 2024. "Effect of BaTiO3 and Chitosan Composite Material on the Enhancement of the Sensitivity and Limit of Detection of the Surface Plasmon Resonance Sensor-Divergent Beam Based". *East African Journal of Information Technology* 7 (1), 412-426. https://doi.org/10.37284/eajit.7.1.2463.

HARVARD CITATION

Hossea, J. H. (2024) "Effect of BaTiO3 and Chitosan Composite Material on the Enhancement of the Sensitivity and Limit of Detection of the Surface Plasmon Resonance Sensor-Divergent Beam Based", *East African Journal of Information Technology*, 7(1), pp. 412-426. doi: 10.37284/eajit.7.1.2463.

IEEE CITATION

J. H., Hossea "Effect of BaTiO3 and Chitosan Composite Material on the Enhancement of the Sensitivity and Limit of Detection of the Surface Plasmon Resonance Sensor-Divergent Beam Based.", *EAJIT*, vol. 7, no. 1, pp. 412-426, Nov. 2024.

MLA CITATION

Hossea, Jordan H "Effect of BaTiO3 and Chitosan Composite Material on the Enhancement of the Sensitivity and Limit of Detection of the Surface Plasmon Resonance Sensor-Divergent Beam Based". *East African Journal of Information Technology*, Vol. 7, no. 1, Nov. 2024, pp. 412-426, doi:10.37284/eajit.7.1.2463.

Article DOI: https://doi.org/10.37284/eajit.7.1.2463

INTRODUCTION

The optical technique of surface plasmon resonance spectroscopy operates on the principle of attenuated total internal reflection (ATR). When P-polarized light illuminates the prism-metal interface at an angle greater than the critical angle, the entire light is reflected, a phenomenon known as total internal reflection [1, 2]. Even if all the light is reflected, a propagating wave known as an evanescent wave will occur at the metal-dielectric interface, which is extremely sensitive to slight changes in the refractive index of the dielectric material [1, 2]. Consequently, surface plasmon resonance occurs when the evanescent wave's propagation constant equals that of the surface plasmon wave [2]. As a result, when the refractive index at the metal-dielectric interface changes, total internal reflection disappears. This is known as attenuated total internal reflection (ATR). The resonance angle is the reflected angle at which the reflected intensity is nearly zero [1, 2]. The detected intensity is indicated by the dark band at this location. When the detected intensity is zero signify optimal photon energy transformation have been achieved.

Researcher have used SPR sensor in many fields like detecting waterborne and airborne harmful bacteria and virus which are dangerous for public health [3, 4]. Quantization of kinetic and equilibrium characterization of biomolecular interactions are easily measured by SPR sensor [5]. Despite the researcher's efforts to improve sensitivity and limit of detection (LOD) in conventional prism based SPR sensors (single metal layer system) that work on angular interrogation, the sensor still suffers from insufficient sensitivity and LOD, despite the fact that high sensitivity and LOD is the primary goal of the researcher. Therefore, recently researchers have shifted their focus to multilayer SPR based as an alternative mechanism of improving the sensitivity and LOD of the SPR sensor.

The designed SPR sensor used Kretschmann based configuration with six layers. Silver as a metal was selected because it has high detection accuracy in comparison to other metals like gold [6]. The adhesion between glass and metal is typically poor because of this, chromium (Cr) and titanium (Ti) are frequently used to increase the adhesion between metal and glass [7]. These materials' low optical transmission and metal interdiffusion limitations are a drawback due their refractive index in visible range has real and imaginary, imaginary part absorb fraction of the photon energy resulting to decrease in sensitivity and widening of the reflected SPR reflectivity curve [7].

The use of the adhesion layer with the real refractive index was an option for improving the sensitivity and detection accuracy [8]. Many studies have proposed the use of Si, SiO_2, ZnO and TiO_2 which gives better SPR performance than those with complex refractive index in the visible [8-10]. However, it has been experimented that the combination of low and high purely real refractive index makes the composite layer of ZnO and TiO_2 produce better sensitivity than single adhesion layer [9, 11].

When silver used in SPR sensor gives better performance than gold in terms of sensitivity and detection accuracy because the ratio of real part to imaginary part of silver is higher than other metals like gold, copper, aluminium and palladium [12]. However, silver has a detrimental effect of easily oxidized when encounter with water, it is hardly to be reused. The researchers have addressed the problem by adding transition metal dichalcogenides (TMDCs) monolayers such as graphene, molybdenum disulfide (MoS_2) [13] with the sensitivity of 230.66°/RIU, $MoSe_2$ [14] with sensitivity of (215.5°/RIU), MXene [15, 16] which are resistant to oxidation, meanwhile the sensitivity is improved.

$BaTiO_3$ is widely used due high purely real refractive index when compared to other transition metal dichalcogenides (TMDCs. Recently research have shown that when transition metal dichalcogenides (TMDCs) combined perovskite material like barium titanate ($BaTiO_3$) the sensitivity of the SPR sensor will be highly improved. It has been observed that $BaTiO_3$ is widely used compared to other

Article DOI: https://doi.org/10.37284/eajit.7.1.2463

perovskite material like, lead titanate ($PbTiO_3$) [17], strontium titanate $SrTiO_3$ and potassium niobate ($KNbO_3$) [18] this is because of due high purely real refractive index [19].

Wang et al. proposed an SPR sensor with a maximum sensitivity of 294°/RIU in a (prism/Ag/Au/$BaTiO_3$/Graphene) configuration structure [20]. Wang et al. [21] present another work in which they design an SPR sensor with a multilayer structure of (Ag/$BaTiO_3$/Graphene) and a sensitivity of 257°/RIU. Saharia et al [22] proposed an SPR sensor sandwiched with ($BaTiO_3$) and graphene that has a sensitivity of 116.67 ˚/RIU. Pal and Jha [23] proposed SPR multilayer (Ag/$BaTiO_3$/Ag/Graphene) sensor with sensitivity of 280˚/RIU. Imam et al [24] proposed calcium fluoride prism/$BaTiO_3$/Blue Phosphorus/WS_2 multilayer structure obtain maximum sensitivity of 413.7 ˚/RIU.

In this article the SPR sensor was configured as calcium fluoride prism CaF_2/ZnO/TiO_2/Ag/ $BaTiO_3$/chitosan. Prism CaF_2 was opted since it has the lowest refractive index which results in high sensitivity and improved LOD compared to the prism with higher refractive index. Apart from prevention of oxidation on the silver, this study has found that optimum thickness of $BaTiO_3$ enhances the sensitivity by the factor of 1.7 in comparison to convection SPR sensor [25]. For the purposes of increasing absorption chitosan film was added on top to $BaTiO_3$ which has high absorption capability [26]. Chitosan is the copolymer which can be formed naturally in some microorganisms such as fungi and yeast [27, 28]. It is biodegradable and harmless to human health. It has numerous applications in food and agriculture technology, biomedicine and cosmetic [27, 29]. Moreover, it can be derived from alkaline N-deacetylation which is mostly found in shells of shrimps, krill, lobsters, and crabs [27]. This signify that chitosan is healthy and easily found. Henceforth, it has low cost. Chitosan has reasonable absorption capacity due to the presence of amine group and hydroxyl group [28, 29]. Therefore, the presence of amine group is helpful for immobilizing the surface which increases carboxylic bonding [30].

Significant effort has been dedicated to improving the sensitivity and limit of detection (LOD) of the SPR sensor using an additional multilayer approach, which are essential attributes for identifying tiny changes in the measured sample. Nevertheless, no theoretical studies have employed a $BaTiO_3$ and Chitosan alloy with appropriate thickness to enhance the sensitivity and detection limit of the SPR sensor. Thus, study concluded that the integration of an optimal chitosan thickness, alongside a suitable $BaTiO_3$ thickness, significantly improved sensitivity and limit of detection (LOD), exceeding the findings of the latest published research in these metrics. The results were realized by using transfer matrix method with help of MATLAB software [2].

THEORETICAL DEVELOPMENT SPR SENSOR

The evanescent wave's vector along the horizontal axis can be represented as follows.

$$K_x = \frac{2\pi}{\lambda} n_p \sin\theta_i \tag{1}$$

where n_p is the prism RI, λ is the wavelength of the light source and θ_i in the incidence angle at prism/metal interface

Article DOI: https://doi.org/10.37284/eajit.7.1.2463

Figure 1: Conventional SPR sensor

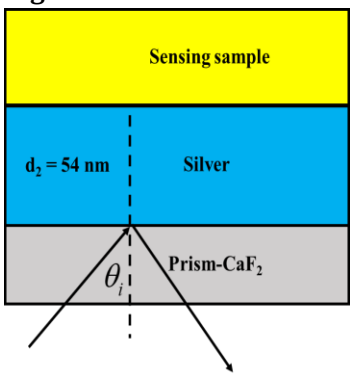

When there is an oscillation of surface charges on the gold layer, the surface plasmon wave vector K_{sp} [8] can be expressed as

$$K_{sp} = \frac{2\pi}{\lambda}\sqrt{\frac{n_{silver}^2 n_{sample}^2}{n_{silver}^2 + n_{sample}^2}}, \qquad (2)$$

Here, n_{silver} and n_{sample} are refractive indices of the silver and dielectric sample respectively. Therefore, (2) show how the horizontal wave vector of metal oscillating electron charges is impacted by changes in refractive index. For the plasmons to resonate and produce the resonance angle, the two wave vectors must coincide.

$$\theta_{spr} = \sin^{-1}\left[\frac{1}{n_p}\sqrt{\frac{n_{silver}^2 n_{sample}^2}{\left(n_{sillver}^2 + n_{sample}^2\right)}}\right]$$

(3)

SPR sensor design considerations, mathematical models' performance measurement parameters

SPR sensor design considerations

Figure 2 illustrates a six-layers structure of the SPR when the p-polarized light with wavelength λ incident on the prism. To prevent mechanical translation or movement, the collimated source is routed through the Powell lens, which diverges the laser beam so that the beam incident on the prism-ZnO contact covers the RI measurement range of 1.3317 to 1.34. The redesigned structure of the SPR sensor is proposed by stacking the layers of different materials along the z-axis. This work's CaF_2 prism has a refractive index of 1.4329, which is lower than BK7 and FK51a's refractive indexes of 1.5151 and 1.4853, respectively. It has been demonstrated that SPR sensors that use prisms with low RI have higher sensitivity. The RI of CaF_2 is calculated using [31]

$$n_{CaF_2} = \left(1 + \frac{0.567588\lambda^2}{\lambda^2 - 0.050263^2} + \frac{0.4710914\lambda^2}{\lambda^2 - 0.10039^2} + \frac{3.8484723\lambda^2}{\lambda^2 - 34.64904^2}\right)$$

(4)

The stacked layers consist of CaF_2/ZnO/TiO_2/Silver/$BaTiO_3$/Chitosan/sensing sample as shown in the **Figure 2**. The thickness of ZnO, TiO_2, silver, $BaTiO_3$ and Chitosan is d_2, d_3, d_4, d_5 and d_6 and their corresponding refractive index shown in **Table 1**. The reflected beam from prism – ZnO interface is reflected to other side of the prism. The refractive index of ZnO can be computed as [32]

$$n_{ZnO} = \sqrt{\left(2.81418 + \frac{0.87968\lambda^2}{\lambda^2 - 0.3042^2} - 0.00711\lambda^2\right)}$$

(5)

Therefore, the reflected intensity can be captured by either a charge couple device (CCD) or complementary metal-oxide (CMOS) sensor. From composite structure **Figure 2** in which an angle θ_i is higher than a critical angle this ensures total internal reflection occurs hence the evanescent wave is generated at prism/ZnO interface which responsible for detecting changes in the sample at chitosan/sample interface. The beam used is diverged beam by using Powell lens

Article DOI: https://doi.org/10.37284/eajit.7.1.2463

which cover entire measurand (1.3317 – 1.34) without any mechanical scanning.

Figure 2: Proposed of a six-layers SPR sensor.

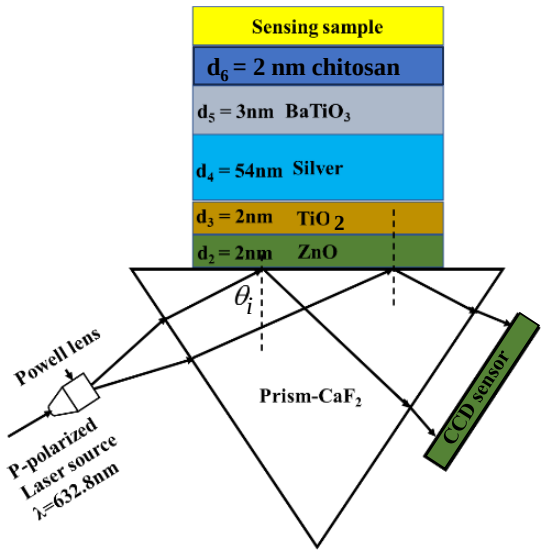

Table 1 shows optical properties material used in the proposed SPR sensor as per provided references.

Table 1: Optical and physical parameters used in the designing of the proposed SPR sensor.

Number of layers	Used material	The refractive index of the material at 632.8 nm	Thickness (nm)	References
1	Prism (CaF_2)	1.4329	-	[31]
2	ZnO	1.98	$d_2 = 2$	[32]
3	TiO_2	2.5837	$d_3 = 2$	[33]
4	Silver	0.05626+4.2776i	$d_4 = 54$	[34]
5	$BaTiO_3$	2.4042	$d_5 = 3$	[35]
6	Chitosan	1.54+0.015i	$d_6 = 2$	[36]
7	Analyte	1.3317 – 1.34	-	

SPR sensor mathematical model for multilayers

The SPR reflectivity curve was calculated in this study using the matrix method [2] on MATLAB software. According to the boundary condition, the electric and magnetic fields, U_1 and V_1, at the first layer's boundary are related to those U_6 and V_6 at the last layer's interface, respectively, by

$$\begin{bmatrix} U_1 \\ V_1 \end{bmatrix} = M \begin{bmatrix} U_6 \\ V_6 \end{bmatrix}, \quad (6)$$

where M is the matrix representing the wave propagation response through different layers by

$$M_{ij} = \prod_{k=2}^{6} \begin{pmatrix} \cos\beta_k & -(i/q_k)\sin\beta_k \\ -iq_k \sin\beta_k & \cos\beta_k \end{pmatrix}_{ij} = \begin{pmatrix} M_{11} & M_{12} \\ M_{21} & M_{22} \end{pmatrix}. \quad (7)$$

Here, the factor q_k is defined as

$$q_k = \frac{\left(n_k^2 - \left(n_p \sin\beta_i\right)^2\right)^{1/2}}{n_k^2}, \quad (7)$$

while β_k is the phase shift of k^{th} layer with a thickness d_k

Article DOI: https://doi.org/10.37284/eajit.7.1.2463

$$\beta_k = \frac{2\pi d_k}{\lambda}\left(n_k^2 - n_p^2 \sin^2\theta_i\right)^{1/2} \quad (8)$$

As the result of the wave propagation through multilayer media, the total reflection coefficient for the transverse magnetic field is expressed by

$$r^{TM} = \frac{\left(M_{11} + M_{12}q_{sample}\right)q_1 - \left(M_{21} + M_{22}q_{sample}\right)}{\left(M_{11} + M_{12}q_{sample}\right)q_1 + \left(M_{21} + M_{22}q_{sample}\right)} \quad (9)$$

with

$$q_{sample} = \frac{\left(n_{sample}^2 - \left(n_p \sin\theta_i\right)^2\right)^{1/2}}{n_{sample}^2} \quad (10)$$

Finally, the reflectivity power can be calculated as

$$R = \left|r^{TM}\right|^2 \quad (11)$$

SPR sensor measurement parameters

The SPR sensor measurement parameters were extracted from the resonance curve, in which sensitivity, detection accuracy and quality factor.

Sensitivity

Sensitivity of the SPR biosensor is measured as change in resonance position in the reflectance curve ($\Delta\theta res$) corresponding to the small change in the refractive index (Δns) of the analyte. The sensitivity is given as[37, 38]

$$S = \frac{\Delta\theta_{res}}{\Delta n_s} \quad (12)$$

Detection Accuracy

DA is inversely proportional to the full width at half maxima (FWHM) of the reflectance curve and is given by[37, 38],

$$DA = \frac{1}{FWHM} \quad (13)$$

Quality Factor (QF)

QF is defined as the ratio of S to the FWHM [37-39], and has unit of RIU^{-1}

$$Q = \frac{S}{FWHM} \quad (14)$$

Limit of detection (LOD)

LOD is the minimum value in which CCD sensor can detect the change of the sample. This parameter depends on angular resolution and the sensitivity of the SPR sensor. Consider the theoretical use imbedded linear array TCD1304AP CCD number of pixel $\left(N_{pixel}\right)$ of 3648 pixels. The controller for the CCD sensor is STM32F401RE microcontroller which has 12-bit ADC converter.

$$LOD\left(\sigma_{RI}\right) = \frac{\sigma_s}{Sensitivity} \quad (15)$$

Where σ_s is the angular resolution of the SPR sensor. σ_s depends on the pixel range covered by resonance angle and the ADC conversion resolution $1/\left(2^n - 1\right)$ is multiplied by the resolution of the CCD. The resolution of the CCD sensor is the minimum angle at which CCD sensor can track changes in one pixel is computed as

$$\sigma_s = \frac{\Delta\theta_{res}}{N_{pixel}} \times \frac{1pixel}{\left(2^n - 1\right)} \quad (16)$$

N_{pixel} is the total number of pixels of CCD sensor and n is the number of bit of ADC converter

Sensor merit

Sensor merit is the parameter which relates the broadening and minimum dip of the SPR reflectivity curve. The broadening of SPR reflectance dip, is quantified by combining the effect of the resolution of the sensor and FWHM and shape of resonance damping in the

Article DOI: https://doi.org/10.37284/eajit.7.1.2463

neighborhood of the minimum. Therefore, sensor merit is expressed as [40-43],

$$SM = \frac{R_{max} - R_{min}}{FWHM} \quad (17)$$

Combined sensitivity factor

Combined sensitivity factor (CSF), is the product of the sensitivity sensor merit (SM) in this work [41, 42]. In [43], it was shown that the aforementioned CSF is inversely proportional to the refractive index resolution and can be written Finally, the CSF is given by S multiplied by SM [40, 43] where the unit is RIU^{-1} and is expressed as:

$$CSF = S \times SM \quad (18)$$

The performance parameters indicate how good the performance of the SPR biosensor is. Note that the behavior of the performance parameters is analyzed with respect to the variation of the chemical potential of graphene

RESULTS AND DISCUSSIONS

Figure 3 depicts reflectance curves for an SPR sensor plotted against incidence angle for various refractive indices (n-s1 = 1.3317 and n-s2 = 1.34) and chitosan thicknesses (1, 2, 3, and 4 nm). The solid lines reflect the case where n-s1 = 1.3317, whereas the dashed lines represent n-s2 = 1.34. As the refractive index grows from 1.3317 to 1.34, the reflectivity dip goes towards higher angles, suggesting a shift in the resonance angle caused by the change in refractive index. [44, 45]. As the thickness increases from 1 nm to 4 nm for both refractive indices, the resonance dip becomes shallower, while the reflectivity curve broadens and shifts slightly. Thicker layers provide broader reflectivity minima, which affects resolution (detection accuracy). All curves show a characteristic drop in reflectivity, corresponding to the resonance state where SPR occurs. This dip is more evident for thinner layers and gets less sharp as the thickness grows, showing a trade-off between detection accuracy and layer thickness [46]. The plot highlights the importance of layer thickness and refractive index in determining the performance of an SPR sensor, with significant implications for the sensitivity and resolution of detection [45].

Figure 3: Shows the SPR reflectivity with variation of the chitosan thickness by 1 nm, 2 nm, 3 nm, and 4 nm on

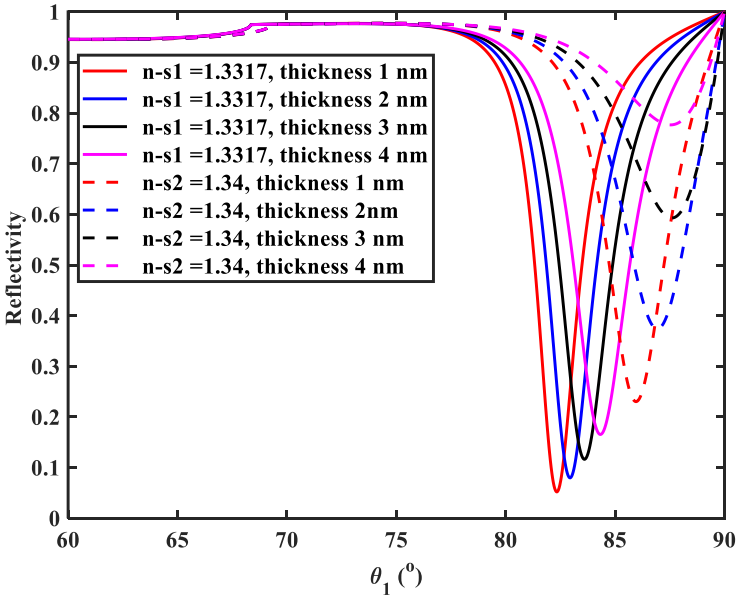

Article DOI: https://doi.org/10.37284/eajit.7.1.2463

The **Figure 4** shows the sensitivity of a SPR sensor as a function of the chitosan layer thickness for different thicknesses of a $BaTiO_3$ layer (1 nm, 2 nm, 3 nm, and 4 nm). The **Figure 4** shows that when the thickness of the chitosan increases the sensitivity increases only when thickness of $BaTiO_3$ is less than 3 nm. As it is clearly shown that when the chitosan thickness of increase from 1 nm to 2 nm the sensitivity also increases from 436.02 to 480.48°/RIU, which implies that the sensitivity improved by 10.20 %. However, when the chitosan thickness increases to 3 nm the sensitivity slightly dropped to 480.36°/RIU, this signify the optimum thickness of chitosan is 2 nm in which high highest sensitivity is achieved. For 1 nm thickness of $BaTiO_3$ (black line) the sensitivity remains fairly constant around 300 °/RIU as the chitosan thickness increases from 1 to 4 nm. For 2 nm thickness of $BaTiO_3$ (red line), the sensitivity gradually increases from about 350 °/RIU to around 400 °/RIU as the chitosan thickness increases. This suggests that an intermediate chitosan thickness, in conjunction with a moderate $BaTiO_3$ layer, provides the best sensitivity for the SPR sensor.

For 4 nm thickness of $BaTiO_3$ (purple line) the sensitivity sharply decreases from around 350 °/RIU at 1 nm of chitosan to almost 0 °/RIU at the range 3 to 4 nm of chitosan, indicating a rapid loss of sensor sensitivity with increasing chitosan thickness for this configuration due to the damping effect of the chitosan as it becomes thicker [46, 47]. This suggests that when the $BaTiO_3$ layer becomes too thick, the sensor's ability to detect changes in refractive index is diminished, possibly due to the reduced interaction of the evanescent field with the sensing medium [46, 47].The impact of chitosan thickness in most configurations (except for the 4 nm $BaTiO_3$ increasing the chitosan thickness enhances the sensitivity, up to a certain limit. This indicates that the chitosan layer plays a significant role in enhancing the sensor's plasmonic response, but beyond a certain thickness, its benefit may diminish or even become detrimental, as seen in the 4 nm $BaTiO_3$.

Figure 4: Shows the effects of increasing the thickness of the $BaTiO_3$ layer by 1 nm, 2 nm, 3 nm, and 4 nm on sensitivity

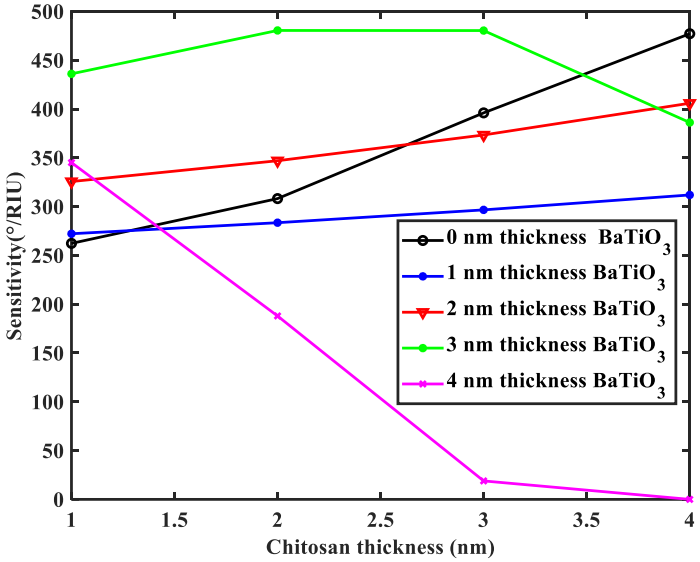

The **Figure 5** shows the minimum dip and FWHM of a SPR sensor as a function of the chitosan layer thickness for different thicknesses of a $BaTiO_3$ layer (1 nm, 2 nm, 3 nm, and 4 nm). The **Figure 5(a)** shows that when the thickness of the chitosan and $BaTiO_3$ increases the minimum dip is getting shallow and shallow decreases only when thickness of $BaTiO_3$ is less than 3 nm. The similar was followed by FWHM as shown in **Figure 5(b**). The broader FWHM leading to poorer detection

Article DOI: https://doi.org/10.37284/eajit.7.1.2463

accuracy for the sample which are very close to each other in terms of refractive index. In which at the thickness of 2 nm the FWHM is around 3.18˚. This yielded as the results of decreasing the evanescent field strength hence reduction in the penetration depth to the measured sample. When the thickness of the chitosan is 2 nm the minimum dip is around 0.22 which implies that optical coupling efficiency is around 78 % which is acceptable value where detection of the minimum dip is possible. Also, at that thickness the maximum sensitivity of 480.4819 is achieved (see **Figure 4**).

Figure 5: Shows the effects of increasing the thickness of the $BaTiO_3$ layer by 1 nm, 2 nm, 3 nm, and 4 nm on (a) Minimum dip and (b) full width at half maximum (FWHM)

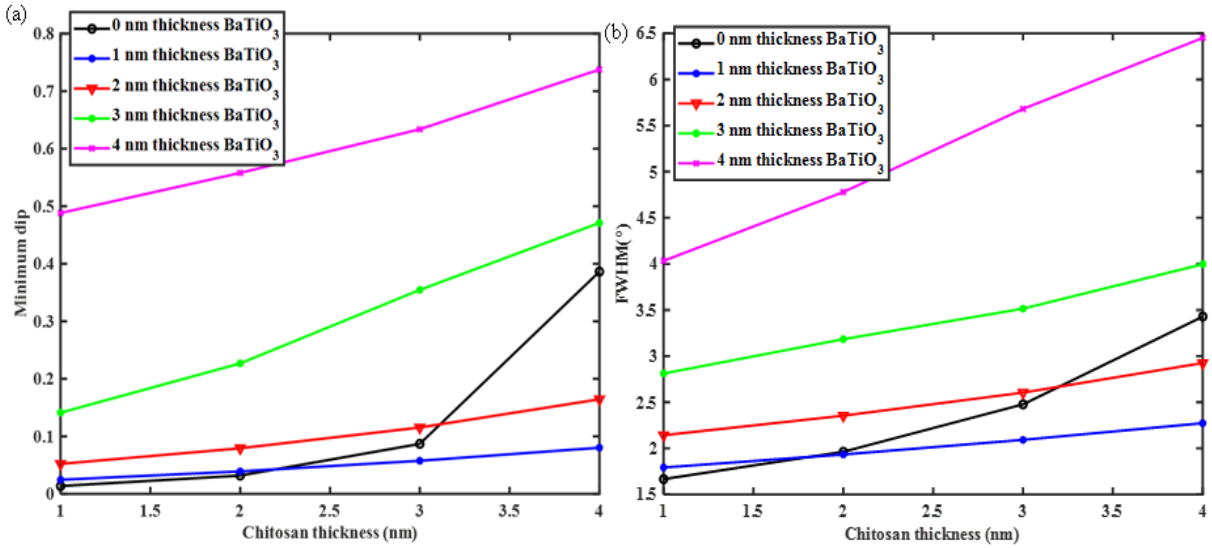

The **Figure 6** shows the detection accuracy and quality factor (QF) of a SPR sensor as a function of the chitosan layer thickness for different thicknesses of a $BaTiO_3$ layer (1 nm, 2 nm, 3 nm, and 4 nm). The variation trend for DA and QF is similar because DA is proportional to QF, since $DA = QF \times \Delta n_s$ in which Δn_s is constant for which is 0.0083 (1.34 – 1.3317). When the thickness of $BaTiO_3$ is less than 3 nm, it is observed that as the chitosan increases up to 3 nm the both DA and QF increases. However, beyond 3 nm of the chitosan and when the thickness of $BaTiO_3$ is more than 3 nm it clearly seen that the both DA and QF decreases. The **Figure 6(a)** shows that when the thickness of the chitosan increases the detection accuracy (DA) decreases since DA is inversely proportional to FWHM while the quality factor (QF) is decreases which the thickness of $BaTiO_3$ is higher than 2 nm. While when the thickness of $BaTiO_3$ is below 2 nm the QF increase with the increase of the thickness of chitosan. When the thickness of $BaTiO_3$ is more than 3 nm the evanescent field strength penetrated into the sample is reduced as results of the thickness. But when there is no it is seen that the detection accuracy and QF is decreases this implies the proper interfacial bonding between the chitosan and $BaTiO_3$ layers plays great role in determining detection accuracy and QF. When the thickness of $BaTiO_3$ is 1 nm it is observed that the both detection accuracy and QF increases which signifies the right proportion for bonding between the chitosan and $BaTiO_3$ adversely the sensitivity is low for thickness. In comparison with other related work the results for DA of our proposed sensor is higher than those published recently [48] [49] [50] and QF (150.88 RIU^{-1}) is higher than [51] which is 118.4 RIU^{-1} and [52] which is 88.84 RIU^{-1}.

Article DOI: https://doi.org/10.37284/eajit.7.1.2463

Figure 6: Shows the effects of increasing the thickness of the $BaTiO_3$ layer by 1 nm, 2 nm, 3 nm, and 4 nm on (a) the detection accuracy (DA) and (b) quality factor (QF).

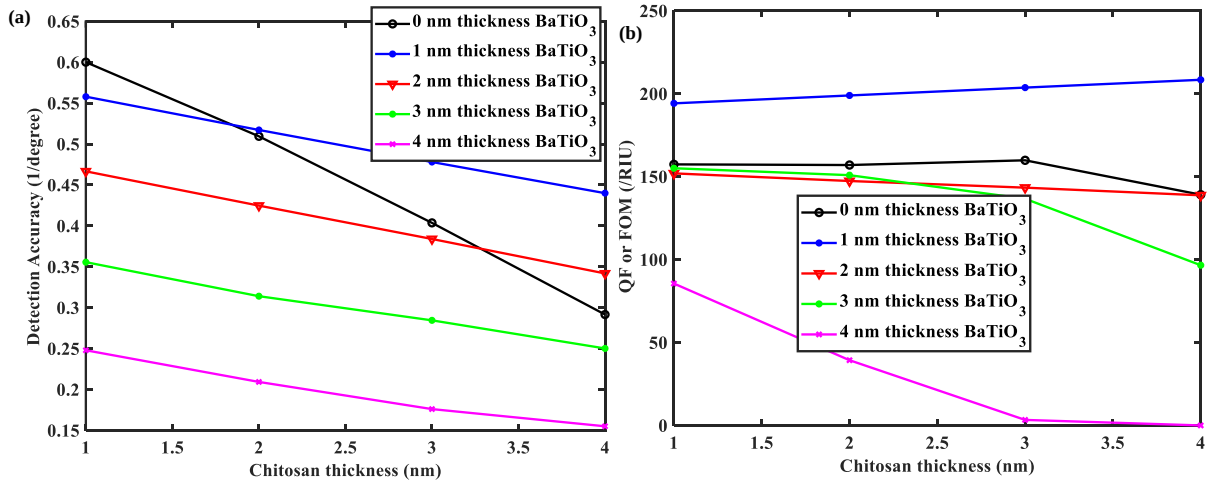

The **Figure 7** shows the SM and CSF of a SPR sensor as a function of the chitosan layer thickness for different thicknesses of a $BaTiO_3$ layer (1 nm, 2 nm, 3 nm, and 4 nm). The variation trend for SM varies in inversely proportional FWHM and proportional to power photon transfer efficiency $(R_{max} - R_{min})$, which implies that the dipper the minimum the higher SM, while the narrower the FWHM the higher SM. From **Figure 7** is clearly seen that as the thickness of chitosan increases the lower the value of SM and CSF.CSF is proportional to the product of sensitivity and SM, thus the higher SM and S the better CSF. When the thickness of $BaTiO_3$ is less than 3 nm, it is observed that as the chitosan increases up to 3 nm the both DA and QF increases. Decrease in both SM and CSF as the chitosan increases caused by reduction of the penetration depth of evanescent was as the chitosan becomes thicker. Also, it is observed that as $BaTiO_3$ thickness increases SM and CSF decreases because of the reduction of evanescent field strength.

Figure 7 Shows the effects of increasing the thickness of the $BaTiO_3$ layer by 1 nm, 2 nm, 3 nm, and 4 nm on (a) Sensor merit (SM) and (b) Combined sensitivity factor (CSF)

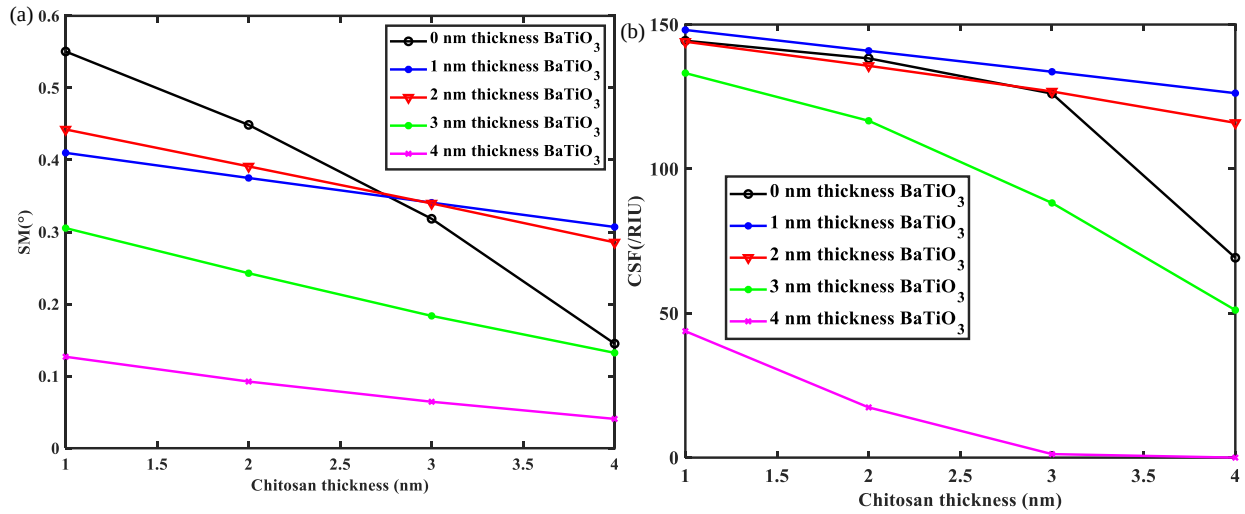

In general, the optimum performance of the SPR sensor was obtained when the thickness of $BaTiO_3$ is 3 nm while the thickness of chitosan is 2 nm. The overall results performance can be summarized as shown in the **Table 2.** The theoretical resolution of the proposed SPR sensor is computed by considering the range of the

Article DOI: https://doi.org/10.37284/eajit.7.1.2463

resonance angle is 3.988˚ which means from 82.939 to 86.927˚ as shown in **Figure 3.**

$$\sigma_s = \frac{3.988^{\circ}}{3648\,pixel} \times \frac{1\,pixel}{4095} = \frac{3.988^{\circ}}{14938560} = 2.6696 \times 10^{-7^{\circ}} \quad (19a)$$

$$LOD(\sigma_{RI}) = \frac{2.6696 \times 10^{-7^{\circ}}}{480.482^{\circ}/RIU} = 5.5561 \times 10^{-10}\,RIU \quad (19b)$$

Therefore, the limit of detection LOD of the proposed SPR sensor has improved from $8.3790 \times 10^{-10}\,RIU$ [25] to $5.5561 \times 10^{-10}\,RIU$. Thus, the limit of detection LOD of the proposed SPR sensor has improved by 33.69 %.

Table 2: An overview of the optimal performance parameters of the proposed SPR sensor.

Parameters	S (°/RIU)	FWHM (degree)	Minimum dip	DA (1/degree)	SM (1/degree)	CSF (1/RIU)	QF (1/RIU)
1	480.482	3.18	0.227	1.25	0.24	116.67	150.88

Comparison of the Proposed SPR Sensor with Recent Publications Pertaining to $BaTiO_3$

Table 2 contrasts the effectiveness of the proposed SPR sensors with that of recently published research. The findings demonstrate that the suggested SPR sensor surpasses a recently published study on sensitivity (S), detection accuracy (DA), and figure of merits (FOM), all of which are essential attributes for detecting analytes with refractive index values ranging from 1.3317 to 1.34. The sensitivity of the proposed SPR sensor is improved by the factor of 1.2 when chitosan of 2 nm was added on top of $BaTiO_3$ [25]. Meanwhile the DA and FOM of the proposed SPR sensor is lowered by the factor of 1.47 and 1.2, respectively, compared to the to the SPR structure without chitosan layer [25]. However, in this application the most important parameters are sensitivity and limit of detection of the SPR sensor which outperform the recently published paper.

Table 2: A comparative study of the proposed SPR sensor and most recently published research work in terms of sensitivity (S), detection accuracy (DA) and Quality factor (QF).

Reference	Reported Year	Structure	Sample range	S (deg./RIU)	DA	FOM or QF (deg./RIU)
[24]	2022	CaF_2/$BaTiO_3$/Blue Phosphorus/WS_2	1.365 - 1.388	413.7 ˚	-	-
[49]	2023	BK7/Ag/$BaTiO_3$ /Ag/Graphene	1.33 - 1.39	220.83	0.819	102.45
[53]	2023	Ag/$BaTiO_3$/ Ag/ WS_2	1.368 -1.392	253.5	0.576	146.02
[54]	2023	Ag/$BaTiO_3$/ Ag_1/ MoS_2	1.368 -1.392	290.71	0.346	100.59
[51]	2023	BK7/Ag/ $BaTiO_3$/Blue P/ MoS_2/WS_2	1.33 -1.335	326	-	-
[48]	2023	CaF_2/Copper /$BaTiO_3$/Graphene	1.33 - 1.34	219	0.47	102.93
[55]	2023	BK_7/Ag/$BaTiO_3$/Graphene	TB	300. 83	0.249	74.91
[50]	2024	BK7/Ag/ $BaTiO_3$/ $MoSe_2$	1.371, 1.41,1.378	247.813	0.17437	43.211
[25]	2024	CaF_2/TiO_2/Ag/$BaTiO_3$	1.3317 -1.34	399.45	0.4606	183.98
	Proposed	**CaF_2/ZnO/TiO_2 /Ag/$BaTiO_3$**	**1.3317 -1.34**	**480.48**	**0.314**	**150.88**

Article DOI: https://doi.org/10.37284/eajit.7.1.2463

CONCLUSION

The designed SPR sensor, enhanced by a chitosan layer above the $BaTiO_3$, has demonstrated improvements in sensitivity and detection accuracy by factors of 16.67 % and 33.69 %, respectively. The enhancement resulted from the precise optimization of the thickness of $BaTiO_3$ and chitosan, with optimal sensitivity and limit of detection (LOD) achieved at a $BaTiO_3$ thickness of 3 nm and a chitosan thickness of 2 nm. The suggested SPR sensor can detect minute variations in the measuring sample within the range of 1.3317 to 1.34 without mechanical rotation. The high sensitivity and low limit of detection (LOD) of 480.45˚/RIU and $5.5561\times10^{-10}\,RIU$, respectively, results in the ability to detect even little variations in measuring samples.

Acknowledgements

The author would like to thank the Dar es Salaam Institute of Technology (DIT) for supporting this study.

REFERENCES

1. Fu, H., et al., Graphene enhances the sensitivity of fiber-optic surface plasmon resonance biosensor. IEEE Sensors Journal, 2015. **15**(10): p. 5478-5482.
2. Shalabney, A. and I. Abdulhalim, Electromagnetic fields distribution in multilayer thin film structures and the origin of sensitivity enhancement in surface plasmon resonance sensors. Sensors and Actuators A: Physical, 2010. **159**(1): p. 24-32.
3. Daher, M.G., et al., Surface plasmon resonance biosensor based on graphene layer for the detection of waterborne bacteria. Journal of Biophotonics, 2022. **15**(5): p. e202200001.
4. Filion-Côté, S., et al., Monitoring of bacterial film formation and its breakdown with an angular-based surface plasmon resonance biosensor. Analyst, 2017. **142**(13): p. 2386-2394.
5. Gupta, B.D., A. Pathak, and V. Semwal, Carbon-based nanomaterials for plasmonic sensors: a review. Sensors, 2019. **19**(16): p. 3536.
6. Jha, R. and A.K. Sharma, High-performance sensor based on surface plasmon resonance with chalcogenide prism and aluminum for detection in infrared. Optics letters, 2009. **34**(6): p. 749-751.
7. Siegfried, T., et al., Engineering metal adhesion layers that do not deteriorate plasmon resonances. ACS nano, 2013. **7**(3): p. 2751-2757.
8. Maurya, J.B. and Y.K. Prajapati, Influence of adhesion layer on performance of surface plasmon resonance sensor. IET Optoelectronics, 2018. **12**(4): p. 168-175.
9. Mei, G.S., P.S. Menon, and G. Hegde, ZnO for performance enhancement of surface plasmon resonance biosensor: a review. Materials Research Express, 2020. **7**(1): p. 012003.
10. Das, C.M., et al., Computational modeling for intelligent surface plasmon resonance sensor design and experimental schemes for real-time plasmonic biosensing: A Review. Advanced Theory and Simulations, 2023. **6**(9): p. 2200886.
11. Maurya, J.B., et al., Sensitivity enhancement of surface plasmon resonance sensor based on graphene–MoS2 hybrid structure with TiO2–SiO2 composite layer. Applied Physics A, 2015. **121**(2): p. 525-533.
12. Mitsushio, M., K. Miyashita, and M. Higo, Sensor properties and surface characterization of the metal-deposited SPR optical fiber sensors with Au, Ag, Cu, and Al. Sensors and Actuators A: Physical, 2006. **125**(2): p. 296-303.
13. Sharma, A.K. and A.K. Pandey, Blue Phosphorene/MoS2 Heterostructure Based SPR Sensor With Enhanced Sensitivity. IEEE

Article DOI: https://doi.org/10.37284/eajit.7.1.2463

Photonics Technology Letters, 2018. **30**(7): p. 595-598.

14. Rouf, H.K. and T. Haque, Sensitivity Enhancement of Graphene-MoSe2–Based SPR Sensor Using Ti Adhesion Layer for Detecting Biological Analytes. Plasmonics, 2021. **16**(6): p. 1945-1954.
15. Karki, B., et al., Sensitivity enhancement of refractive index-based surface plasmon resonance sensor for glucose detection. Optical and Quantum Electronics, 2022. **54**(9): p. 595.
16. Almawgani, A.H., et al., Optical detection of fat concentration in milk using MXene-based surface plasmon resonance structure. Biosensors, 2022. **12**(7): p. 535.
17. Cai, W., et al., Preparation and optical properties of barium titanate thin films. Physica B: Condensed Matter, 2011. **406**(19): p. 3583-3587.
18. Singh, S., J. Remeika, and J. Potopowicz, Nonlinear optical properties of ferroelectric lead titanate. Applied Physics Letters, 1972. **20**(3): p. 135-137.
19. Srivastava, A., R. Das, and Y.K. Prajapati, Effect of perovskite material on performance of surface plasmon resonance biosensor. IET Optoelectronics, 2020. **14**(5): p. 256-265.
20. Liu, L., et al., Sensitivity enhancement of a graphene–barium titanate-based surface plasmon resonance biosensor with an Ag–Au bimetallic structure in the visible region. JOSA B, 2019. **36**(4): p. 1108-1116.
21. Sun, P., et al., Sensitivity enhancement of surface plasmon resonance biosensor based on graphene and barium titanate layers. Applied Surface Science, 2019. **475**: p. 342-347.
22. Mudgal, N., et al., ZnO and Bi-metallic (Ag–Au) layers based surface plasmon resonance (SPR) biosensor with BaTiO3 and graphene for biosensing applications. IETE Journal of Research, 2020: p. 1-8.
23. Pal, A. and A. Jha, A theoretical analysis on sensitivity improvement of an SPR refractive index sensor with graphene and barium titanate nanosheets. Optik, 2021. **231**: p. 166378.
24. Ishtiak, K.M., S.-A. Imam, and Q.D. Khosru, BaTiO3-Blue Phosphorus/WS2 hybrid structure-based surface plasmon resonance biosensor with enhanced sensor performance for rapid bacterial detection. Results in Engineering, 2022. **16**: p. 100698.
25. Hossea, J.H. and G. Rugumira, Analytical Design of a Portable Surface Plasmon Resonance Sensor by Using a Divergence Beam for Measuring Multiple Heavy Metals and Other Contamination Simultaneously. East African Journal of Engineering, 2024. **7**(1): p. 148-161.
26. Fouad, S., et al., Enhanced sensitivity of surface plasmon resonance sensor based on bilayers of silver-barium titanate. Журнал нано-та електронної фізики, 2016(8,№ 4 (2)): p. 04085-1-04085-5.
27. Fen, Y.W., et al., Surface plasmon resonance optical sensor for mercury ion detection by crosslinked chitosan thin film. Journal of Optoelectronics and Advanced Materials, 2011. **13**(March 2011): p. 279-285.
28. Nasiri, H. and K. Abbasian, High-sensitive surface plasmon resonance sensor for melamine detection in dairy products based on graphene oxide/chitosan nanocomposite. Food Control, 2024. **166**: p. 110761.
29. Lokman, N.F., et al., Highly sensitive SPR response of Au/chitosan/graphene oxide nanostructured thin films toward Pb (II) ions. Sensors and Actuators B: Chemical, 2014. **195**: p. 459-466.
30. Zhang, Y.-n., et al., Optical fiber sensors for measurement of heavy metal ion concentration: A review. Measurement, 2020. **158**: p. 107742.

Article DOI: https://doi.org/10.37284/eajit.7.1.2463

31. Malitson, I.H., A redetermination of some optical properties of calcium fluoride. Applied Optics, 1963. **2**(11): p. 1103-1107.
32. Bass, M., et al., Handbook of Optics, Volume V: Atmospheric Optics, Modulators, Fiber Optics, X-Ray and Neutron Optics. 2009: McGraw-Hill, Inc.
33. Jorgenson, R.C. and S.S. Yee, A fiber-optic chemical sensor based on surface plasmon resonance. Sensors and Actuators B: Chemical, 1993. **12**(3): p. 213-220.
34. Johnson, P.B. and R.-W. Christy, Optical constants of the noble metals. Physical review B, 1972. **6**(12): p. 4370.
35. Wemple, S., M. Didomenico Jr, and I. Camlibel, Dielectric and optical properties of melt-grown BaTiO3. Journal of Physics and Chemistry of Solids, 1968. **29**(10): p. 1797-1803.
36. Fen, Y.W., et al., Optical properties of crosslinked chitosan thin film with glutaraldehyde using surface plasmon resonance technique. American Journal of Engineering and Applied Sciences, 2011. **4**(1): p. 61-65.
37. Rahman, M.M., et al., Sensitivity enhancement of SPR biosensors employing heterostructure of PtSe2 and 2D materials. Optical Materials, 2020. **107**: p. 110123.
38. Meshginqalam, B. and J. Barvestani, Performance enhancement of SPR biosensor based on phosphorene and transition metal dichalcogenides for sensing DNA hybridization. IEEE sensors Journal, 2018. **18**(18): p. 7537-7543.
39. Karki, B., et al., Titanium dioxide, black phosphorus and bimetallic layer-based surface plasmon biosensor for formalin detection: numerical analysis. Optical and Quantum Electronics, 2022. **54**(7): p. 451.
40. Ceballos-Zumaya, J., et al., Performance parameters as a function of graphene's chemical potential for SPR biosensor based on 2D materials. Optik, 2024: p. 172013.
41. Vlcek, J., J. Pistora, and M. Lesnák. Sensitivity enhancement in surface plasmon resonance sensors: theoretical modeling. in Optical Sensors 2009. 2009. SPIE.
42. Sharma, A.K. and A. Dominic, Influence of chemical potential on graphene-based SPR sensor's performance. IEEE Photonics Technology Letters, 2017. **30**(1): p. 95-98.
43. Anjitha, M., et al., Hybrid Design Architecture and Sensitivity Analysis of Cu Based Surface Plasmon Resonance Sensors. Research Transcripts in Materials, 2021. **1**: p. 17-34.
44. Masson, J.-F., Surface plasmon resonance clinical biosensors for medical diagnostics. ACS sensors, 2017. **2**(1): p. 16-30.
45. Vasimalla, Y., H.S. Pradhan, and R.J. Pandya, Sensitivity enhancement of the SPR biosensor for Pseudomonas bacterial detection employing a silicon-barium titanate structure. Applied Optics, 2021. **60**(19): p. 5588-5598.
46. Singh, T.I., P. Singh, and B. Karki, Early detection of chikungunya virus utilizing the surface plasmon resonance comprising a silver-silicon-PtSe2 multilayer structure. Plasmonics, 2023. **18**(3): p. 1173-1180.
47. Karki, B., et al., PtSe2 and black phosphorus employed for sensitivity improvement in the surface plasmon resonance sensor. Journal of Computational Electronics, 2023. **22**(1): p. 106-115.
48. Sharma, V., L.K. Dwivedi, and S.K. Singh, Graphene-Coated Surface Plasmon Resonance (SPR) Sensor for Detection of Preservatives in Milk: A Theoretical Investigation. 2023.
49. Taya, S.A., et al., A surface plasmon resonance nanostructure containing graphene and BaTiO3 layers for sensitive defection of organic compounds. Royal Society Open Science, 2023. **10**(6): p. 230282.

Article DOI: https://doi.org/10.37284/eajit.7.1.2463

50. Kumar, V., S.K. Raghuwanshi, and S. Kumar. Novel surface plasmon resonance (SPR)-based biosensor for pathogenic bacteria detection (PathoBactD). in Optical Interactions with Tissue and Cells XXXV. 2024. SPIE.

51. Kashyap, R., U.R. Baruah, and B. Mondal. BaTiO 3 and Blue Phosphorus-MoS 2/WS 2 hybrid structure based Surface Plasmon Resonance sensor with improved sensing performance. in 2023 16th International Conference on Sensing Technology (ICST). 2023. IEEE.

52. Yesudasu, V., et al., Surface-Plasmon and Titanate Material-Assisted Sensor Structure for Pseudomonas Bacteria Detection With Increased Sensitivity. IEEE Transactions on AgriFood Electronics, 2024.

53. Kumar, V., S.K. Raghuwanshi, and S. Kumar, Nanomaterial-based surface plasmon resonance sensing chip for detection of skin and breast cancer. Plasmonics, 2024. **19**(2): p. 643-654.

54. Kumar, V., S.K. Raghuwanshi, and S. Kumar, Highly sensitive Ag/BaTiO3/MoS2 nano composite layer based SPR sensor for detection of blood and cervical cancer. Results in Optics, 2024. **14**: p. 100597.

55. Daher, M.G., et al., Optical biosensor based on surface plasmon resonance nanostructure for the detection of mycobacterium tuberculosis bacteria with ultra-high efficiency and detection accuracy. Plasmonics, 2023. **18**(6): p. 2195-2204.

